THE JOURNAL OF BIOLOGICAL CHEMISTRY VOL. 281, NO. 4, pp. 2225–2231, January 27, 2006

Paratope Determination of the Antithrombotic Antibody 82D6A3 Based on the Crystal Structure of Its Complex with the von Willebrand Factor A3-Domain*

Received for publication, July 27, 2005, and in revised form, November 17, 2005 Published, JBC Papers in Press, November 28, 2005, DOI 10.1074/jbc.M508191200

Stephanie Staelens[‡], Michael A. Hadders[§], Stephan Vauterin[‡], Céline Platteau[‡], Marc De Maeyer[¶], Karen Vanhoorelbeke[‡1], Eric G. Huizinga[§], and Hans Deckmyn[‡2]

From the [‡]Laboratory for Thrombosis Research, IRC, KU Leuven Campus Kortrijk, 8500 Kortrijk, Belgium, [§]Crystal and Structural Chemistry, Department of Chemistry, Bijvoet Center for Biomolecular Research, Utrecht University, 3584 CH Utrecht, The Netherlands, and [¶]Laboratory of Biomolecular Modeling, KU Leuven, 3000 Leuven, Belgium

The antithrombotic monoclonal antibody 82D6A3 is directed against amino acids Arg-963, Pro-981, Asp-1009, Arg-1016, Ser-1020, Met-1022, and His-1023 of the von Willebrand factor A3-domain (Vanhoorelbeke, K., Depraetere, H., Romijn, R. A., Huizinga, E., De Maeyer, M., and Deckmyn, H. (2003) *J. Biol. Chem.* 278, 37815–37821). By this, it potently inhibits the interaction of von Willebrand factor to collagens, which is a prerequisite for blood platelet adhesion to the injured vessel wall at sites of high shear. To fully understand the mode of action of 82D6A3 at the molecular level, we resolved its crystal structure in complex with the A3-domain and fine mapped its paratope by construction and characterization of 13 mutants. The paratope predominantly consists of two short sequences in the heavy chain CDR1 (Asn-31 and Tyr-32) and CDR3 (Asp-99, Pro-101, Tyr-102 and Tyr-103), forming one patch on the surface of the antibody. Trp-50 of the heavy and His-49 of the light chain, both situated adjacent to the patch, play ancillary roles in antigen binding. The crystal structure furthermore confirms the epitope location, which largely overlaps with the collagen binding site deduced from mutagenesis of the A3-domain (Romijn, R. A., Westein, E., Bouma, B., Schiphorst, M. E., Sixma, J. J., Lenting, P. J., and Huizinga, E. G. (2003) *J. Biol. Chem.* 278, 15035–15039). We herewith further consolidate the location of the collagen binding site and reveal that the potent action of the antibody is due to direct competition for the same interaction site. This information allows the design of a paratope-mimicking peptide with antithrombotic properties.

Platelet adhesion, activation, and aggregation are the three major steps in primary hemostasis, a process that is necessary for the cessation of bleeding at sites of vascular injury. The same process is also responsible for pathologic thrombus formation, particularly in arteries at sites of high shear stress. At high shear stress, binding of von Willebrand factor (VWF)[3] to collagen that is exposed in the subendothelial matrix after injury, and the subsequent interaction of the immobilized VWF with the platelet glycoprotein (GP) Ib/IX/V-receptor complex, is a prerequisite for proper adhesion (1–3). As a result of the reversible VWF-GP Ib/IX/V interaction, platelets roll over the injured vessel wall and slow down (3). Subsequent firm adhesion and activation of platelets are mediated by their collagen receptors, integrins $\alpha2\beta1$ and GPVI, respectively (4–8). Activated platelets expose high affinity GPIIb/IIIa receptors that mediate aggregation by binding to fibrinogen and, to a lesser extent, to VWF (9–11).

Collagen type VI and fibrillar collagens types I and III are abundant in the subendothelium (12). VWF interacts with the fibrillar collagens mainly via its A3-domain (13, 14), whereas its A1-domain has been implicated in binding to collagen type VI (15, 16). The latter interaction only mediates platelet adhesion under low shear conditions (17, 18). The A3-domain is homologous in sequence and structure with the I-domains of collagen binding integrin α-chains, such as the I-domain of $\alpha2\beta1$ (19–21). These domains adopt a dinucleotide binding fold, or Rossman fold, that consists of a central hydrophobic parallel β-sheet flanked on both sites with amphipathic α-helices (22–24). Despite their structural similarity, they bind collagen in distinctly different ways. The I-domain of $\alpha2\beta1$ binds collagen in a hydrophilic groove at its top face that contains a metal ion-dependent adhesion site (25, 26). In contrast, the collagen-binding site of the A3-domain is located at its front face and is rather flat and hydrophobic (23, 27–29).

Our group characterized a monoclonal antibody against human VWF, 82D6A3, that binds with high affinity to the VWF A3-domain and inhibits VWF binding to collagen types I and III (15). Its inhibiting effect on VWF-mediated platelet adhesion becomes more pronounced with increasing shear stress, as is expected because the collagen-VWF-GPIb axis is essential for platelet adhesion under high shear only (30). The discontinuous epitope of 82D6A3, which has recently been unraveled via phage display and binding studies with alanine mutants of the VWF A3-domain, includes several residues of the A3-domain that are important for collagen binding (30). We further demonstrated that 82D6A3 has antithrombotic effects in a baboon arterial thrombosis model (31), proving for the first time that the VWF-collagen interaction is indeed involved in thrombus formation *in vivo* (32). Interestingly, the antithrombotic effect was not associated with significantly increased bleeding times, even at high doses, demonstrating that administration of 82D6A3 results in a broad therapeutic window. These benefits were also observed in *in vivo* studies with saratin, another inhibitor of the VWF-collagen interaction (33, 34), and with monoclonal antibodies 6B4 (35, 36) and AjvW-2 (37, 38), which inhibit VWF-GPIb binding. This suggests that interference with the collagen-VWF-GPIb axis could have important advantages over existing antithrombotic agents such as

* This study was supported by the Fonds voor Wetenschappelijk Onderzoek-Vlaanderen, Belgium Grant G.0168.02 and IWT-Thromb-X Grant AUT/020473. The costs of publication of this article were defrayed in part by the payment of page charges. This article must therefore be hereby marked "*advertisement*" in accordance with 18 U.S.C. Section 1734 solely to indicate this fact.

The atomic coordinates and structure factors (code 2ADF) have been deposited in the Protein Data Bank, Research Collaboratory for Structural Bioinformatics, Rutgers University, New Brunswick, NJ (http://www.rcsb.org/).

[1] Supported by a postdoctoral fellowship of the Fond voor Wetenschappelijk Onderzoek-Vlaanderen, Belgium.

[2] To whom correspondence should be addressed: Laboratory for Thrombosis Research, IRC, KU Leuven Campus Kortrijk, E. Sabbelaan 53, 8500 Kortrijk, Belgium. Tel.: 32-56-24-64-22; Fax: 32-56-24-69-97; E-mail: Hans.Deckmyn@kuleuven-kortrijk.be.

[3] The abbreviations used are: VWF, von Willebrand factor; GP, glycoprotein; CDR, complementarity-determining region; PBS, phosphate-buffered saline; WT, wild type.

inhibitors of platelet aggregation (GPIIb/IIIa-receptor blockers) or platelet activation (aspirin). Treatment with the latter agents results in smaller therapeutic windows and is frequently associated with bleeding problems and thus requires close monitoring of the patients (39–41). In addition, compounds that interfere with the collagen-VWF-GPIb interaction could also be more effective in the prevention of intimal hyperplasia after angioplasty and endarterectomy, because they interfere with the first steps in primary hemostasis and thus prevent the release of smooth muscle cell mitogenic (*e.g.* transforming growth factor β1) and attractant (*e.g.* basic fibroblast growth factor) factors during platelet activation (42, 43).

The goal of this study was to determine which residues of 82D6A3 are involved in the interaction with the VWF A3-domain. In the future, this information will be used as a lead for the construction of a peptidomimetic with similar inhibitory characteristics as 82D6A3. On the basis of the crystal structure of the complex between 82D6A3 and the VWF A3-domain determined in this study, we selected amino acids of the complementarity-determining regions (CDR) of the antibody for mutation to alanine. Binding studies with alanine mutants of the single chain variable fragment of 82D6A3 (scFv-82D6A3) resulted in the identification of the paratope.

EXPERIMENTAL PROCEDURES

Materials—The pCANTAB 5 E expression vector, pCANTAB 5 E gene rescue primer R2 and horseradish peroxidase (HRP)-labeled anti-E Tag antibodies (anti-E Tag-HRP) were purchased from Amersham Biosciences. Human full-length VWF purified from donor plasma displaying a normal multimeric pattern was purchased from Red Cross, Belgium. Bacti casein peptone, Bacti yeast extract, and Bacti purified agar were purchased from BioTrading (Keerbergen, Belgium). PCR buffer, dNTP, and primers for the construction of the scFv-DNA and for its ligation in the prokaryotic expression vector were purchased from Invitrogen. Primers for the construction of the mutants were purchased from Eurogentec (Seraing, Belgium).

Preparation of VWF A3-domain and Fab Fragments of 82D6A3—Recombinant VWF A3-domain comprising residues 920–1111 of mature VWF was expressed and purified essentially as described (22) with one modification. During removal of the His tag with thrombin the A3-domain precipitated. Resolubilization without significant protein loss was achieved by the addition of solid urea to a final concentration of 7 M followed by overnight dialysis against 25 mM Tris/HCl, pH 8.2. Subsequent purification proceeded as described previously.

82D6A3 was raised in mice against human VWF (15). The IgG of 82D6A3 was purified from earlier produced ascites, and Fab fragments were prepared as previously described (30) and dialysed to 25 mM Tris/HCl, pH 8.2, and 50 mM NaCl.

Crystallization and Data Collection—Crystals of space group $P2_12_12_1$ (unit cell dimensions a = 72.2 Å, b = 89.1 Å, c = 123.5 Å) were obtained using the hanging drop vapor diffusion method. VWF A3-domain (10 mg/ml) and 82D6A3 Fab fragment (7 mg/ml) were mixed in a 1:1 molar ratio and allowed to equilibrate at 21 °C against a reservoir solution containing 12% (w/v) polyethylene glycol 8000, 0.2 M ammonium sulfate, and 0.1 M sodium acetate, pH 4.6. Crystals grew overnight with dimensions of ~0.4 × 0.1 × 0.1 mm.

For data collection, crystals were transferred to reservoir solution supplemented with 20% (v/v) glycerol and flash frozen in liquid nitrogen. Diffraction data were collected at 100 K on beam line ID14 EH4 at the European Synchrotron Radiation Facility (Grenoble, France). Data were collected to 1.9 Å resolution with oscillations of 0.7° to reduce spot overlap. Data were processed using computer programs MOSFLM, SCALA, and TRUNCATE (44, 45). Data collection statistics are found in Table 1.

TABLE 1
Diffraction data and refinement statistics
*, values between parentheses refer to a shell of high resolution diffraction data.

Resolution (Å)	28.4–1.9 (2.0–1.9)*
Completeness (%)	99.9 (100.0)
Redundancy	5.1 (5.2)
R_{sym} (%)	7.4 (26.2)
$I/\sigma I$	15.2 (2.3)
R (%)	18.5 (21.2)
R_{free} (%)	21.7 (25.1)
Root mean square deviation bonds (Å)	0.015
Root mean square deviation angles (°)	1.6

Structure Determination—The structure of the complex of the A3-domain and 82D6A3 was solved by molecular replacement using the program CNS (46). One Fab fragment (47) (Protein Data Bank accession code 2MPA) and one A3-domain (22) (Protein Data Bank accession code 1ATZ) could be oriented and placed in the asymmetric unit. Subsequent rigid body refinement led to an initial model with an *R*-factor of 44.6%. Automatic model building, using the program ARP/wARP (48), built ~80% of the main chain. The model was manually corrected and supplemented in "O" (49). The model was refined with multiple cycles of TLS and restrained refinement using the program Refmac (50, 51), followed by manual rebuilding in "O." Solvent molecules were added to the model automatically using ARP/wARP. Waters were placed in electron difference peaks with a height >3 Σ and were checked manually in "O." Cross-validation, using a 5% test set of reflections, was used throughout refinement. Figures were generated using PyMOL (pymol.sourceforge.net/).

Prokaryotic Expression and Purification of Wild Type scFv of 82D6A3 (scFv-82D6A3(WT))—The construction of scFv-82D6A3(WT) (European Bioinformatics Institute Database accession number AJ965435) through splicing by overlap extension, its cloning in the pCANTAB 5 E vector, and its expression as a soluble protein in the periplasm of *Escherichia coli* HB2151 cells has been previously described (52). The scFv-82D6A3(WT) was purified from the periplasmic extract and the supernatant as described, using a HiTrap anti-E Tag column (RPAS purification module; Amersham Biosciences) (52). After dialysis against PBS, purity was checked in SDS-PAGE using a 10% gel followed by staining with Coomassie Brilliant Blue.

Construction, Expression, and Purification of Alanine Mutants of scFv-82D6A3—Construction of alanine mutants was performed with the QuikChange® site-directed mutagenesis kit (Stratagene) using pCANTAB 5 E-scFv-82D6A3(WT)-DNA and the primers listed in Table 2. The DpnI-digested mutagenesis mixture was immediately used to transform *E. coli* HB2151 cells according to the manufacturer's instructions (RPAS expression module; Amersham Biosciences). Plasmid DNA was prepared using the NucleoSpin® Plasmid Quick Pure kit (Machery-Nagel, Düren, Germany). Sequencing, expression, and purification were performed as described (52). After dialysis against PBS, purity was checked as described above.

Western Blot—Equal volumes of supernatant, periplasm, or elution fractions containing scFv-82D6A3(WT) or its alanine mutants were loaded on a 10% SDS-PAGE gel and transferred to a nitrocellulose membrane (Schleicher & Schuell BioScience, Dassel, Germany). Detection of the scFvs with anti-E Tag-horseradish peroxidase antibodies was performed as described (52).

Concentration Determination of the Purified scFvs—The concentration of the purified scFvs was determined according to the Bradford method (53) using the Coomassie® Plus protein assay kit (Pierce). Briefly, dilution series of purified scFvs and Albumin Standard in PBS

TABLE 2
Oligonucleotide sequence of the primers used for the construction of mutant scFv-82D6A3-DNA

Mutant[a]	Primer[b]
H31Asn → Ala	5′-CA GGG TAT ACC TTT ATA GCT TAT GGA ATG AAC TGG G-3′
H32Tyr → Ala	5′-GGG TAT ACC TTT ATA AAT GCT GGA ATG AAC TGG GTG-3′
H50Trp → Ala	5′-GT TTA AAG TGG ATG GGC GCG AAA AAC ACC AAC ACT GG-3′
H54Asn → Ala	5′-GGC TGG AAA AAC ACC GCC ACT GGA GAG ACA AC-3′
H99Asp → Ala	5-CAT ATT TCT GTG CAA GAG CTA ACC CTT ACT ATG CTT TG-3′
H101Pro → Ala	5′-GT GCA AGA GAT AAC GCT TAC TAT GCT TTG G-3′
H102Tyr → Ala	5′-GCA AGA GAT AAC CCT GCG TAT GCT TTG GAC TAC-3′
H103Tyr → Ala	5′-GCA AGA GAT AAC CCT TAC GCG GCT TTG GAC TAC TGG-3′
L32Tyr → Ala	5′-C CAA GAC ATT AAC AAG GCG ATA GCT TGG TAC CAA C-3′
L49His → Ala	5′-CCT AGG CTG CTC ATA GCT TAC ACA TCT ACA TTA C-3′
L56Pro → Ala	5′-CA TCT ACA TTA CAG GCA GGC ATC CCA TCA AGG-3′
L92Asp → Ala	5′-CT TAT TAT TGT CTA CAG TAT GCG AAT CTT CGG ACG TTC GG-3′
L95Arg → Ala	5′-CAG TAT GAT AAT CTT GCG ACG TTC GGT GGA GG-3′

[a] The name of the constructed alanine mutants with H or L indicating that the mutation is on the heavy or the light chain, respectively, and with the number indicating the position of the residue (first three-letter amino acid code) that is mutated to alanine (Ala) (52).
[b] The sequence of the sense primer, hybridizing with the non-coding strand of scFv-82D6A3-DNA, used for the construction of the mutant. The underlined nucleotides introduce the desired mutation.

were added to a 96-well plate (Greiner, Frickenhausen, Germany). A fixed volume of Coomassie® Plus protein assay reagent was added, and absorbance was measured at 630 nm.

Binding of scFv-82D6A3(WT) and Its Alanine Mutants to VWF—Binding of scFv-82D6A3(WT) and its alanine mutants to VWF was performed as described before (52). Briefly, a 96-well plate was coated with VWF and incubated with dilution series of purified scFv-82D6A3(WT) and its alanine mutants. Next, bound scFv was detected by incubation with anti-E Tag-horseradish peroxidase antibodies. Visualization was performed by adding H_2O_2 and orthophenylenediamine (Sigma). The plate was washed three times after coating and blocking and nine times elsewhere with PBS, 0.1% Tween 20.

Inhibition of the scFv Binding to VWF by IgG-82D6A3—A 96-well plate was coated with VWF, blocked, and incubated as described above with scFv-82D6A3(WT) and its alanine mutants at their respective EC_{50} concentrations as calculated from their binding curves. IgG-82D6A3 (15 μg/ml in PBS, 0.3% milk powder) was added to the plate for 1 h at room temperature. Detection of bound scFv, visualization, and washing were performed as described above.

RESULTS

Structure Determination and Refinement—We solved the crystal structure of the complex between the VWF A3-domain and the Fab fragment of 82D6A3 to 1.9 Å resolution (Fig. 1*A*) (Protein Data Bank accession code 2ADF). The structure has been refined to an *R*-factor of 18.5% and a free *R*-factor of 21.7% and shows good geometry (Table 1). The final model contains residues 922–1110 of the A3-domain, residues 1–210 of the 82D6A3 light chain, and residues 1–216 of the 82D6A3 heavy chain. The electron density of residues 122–130, 152–156, 181–189, and 199–201 in the constant domain of the light chain is ill defined, and the interpretation of these residues is tentative. This does not affect the analysis of the A3–82D6A3 interaction, because these residues are not located in the vicinity of the antigen binding surface of the antibody.

The Epitope of 82D6A3—82D6A3 binds a discontinuous epitope located at a side face of the A3-domain (Fig. 1*B*). The interaction buries a solvent-accessible surface of ~1640 Å^2. The epitope consists of residues located in strand β3, helix α3, and loops β2-β3 and α3-β4. Loop α3-β4 and α3 residue Arg-1016 form a protrusion on the surface of the A3-domain that is nicely accommodated by a cleft between the light and heavy chain subunits of 82D6A3. Accordingly, mutations of Arg-1016 and residues Ser-1020, Met-1022, and His-1023 of α3-β4 led to a significant decrease in binding of VWF to 82D6A3 (30). Residues in the A3-domain implicated in collagen binding, as defined by mutagenesis studies, are located in helix α3, strand β3, and loops α2-α3 and α3-β4

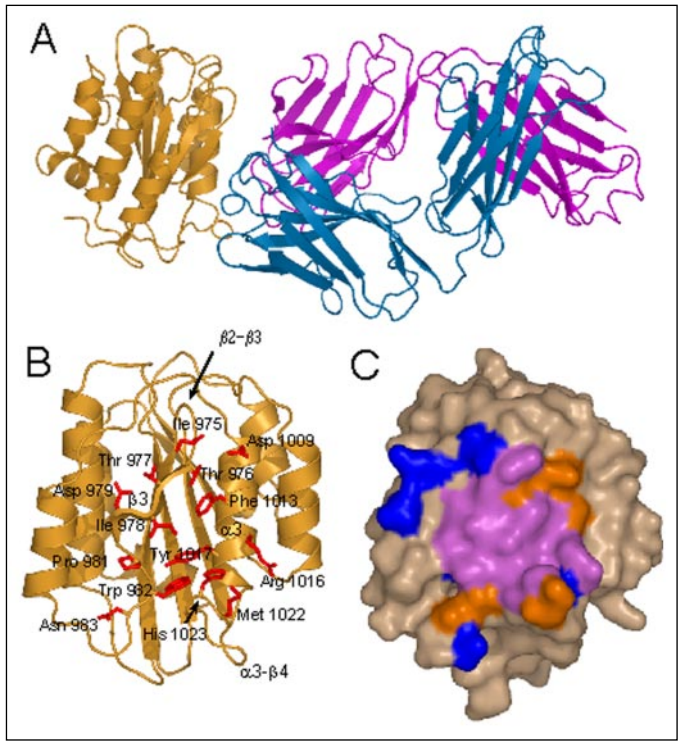

FIGURE 1. **Structure of the complex of the 82D6A3 Fab fragment and the VWF A3-domain.** *A*, ribbon representation of the complex. VWF A3-domain, *yellow*; 82D6A3 heavy chain, *blue*; 82D6A3 light chain, *magenta*. *B*, ribbon representation of the A3-domain with residues that are part of the epitope shown as *red sticks*. *C*, surface representation of the A3-domain with surface area that is involved in both 82D6A3 and collagen binding (colored *purple*), and surface areas exclusively involved in 82D6A3 or collagen binding (colored *orange* and *blue*, respectively). Residues are considered to be involved in 82D6A3 binding if they are within 4 Å of 82D6A3 in the structure of the A3–82D6A3 complex. Residues involved in collagen binding were selected on the basis of the combined results from previous mutagenesis studies (27–29).

(27–29). Although it cannot be excluded that the mutations in the A3-domain have caused indirect effects on collagen binding, these residues define a putative collagen binding surface that overlaps extensively with the footprint of 82D6A3 (Fig. 1*C*), and thus 82D6A3 effectively blocks collagen binding to VWF by direct competition for the same binding site.

82D6A3 Residues Interacting with the A3-Domain—Residues of 82D6A3 that interact with the A3-domain are located in all six CDRs forming five hydrogen bonds and three salt bridges, listed in Table 3, and numerous van der Waals interactions. The heavy chain seems to be the most important in antigen binding with 608 Å^2 of its solvent-acces-

sible surface buried in the complex compared with only 216 Å^2 for the light chain.

As is frequently observed in antigen binding, CDR3 of the heavy chain is involved in many interactions. A salt bridge is present between H99Asp of 82D6A3 and His-1023 of the A3-domain (Fig. 2*A*). Furthermore, H103Tyr interacts through hydrogen bonding with the side chain of Asp-1009 and the main chain nitrogen of Thr-976. Extensive hydrophobic interactions exist between CDR3 residues H101Pro, H102Tyr, and H103Tyr and A3-domain residues Ile-975, Gly-1012, Phe-1013, Arg-1016, and Tyr-1017. In CDR1 the two main interacting residues are H31Asn and H32Tyr (Fig. 2*B*). H31Asn forms hydrogen bonds to the main chain oxygen atoms of Asp-979 and Ile-978 and makes hydrophobic contacts with Pro-981, while H32Tyr forms a hydrogen bond with the main chain nitrogen of Ile-978. CDR2 contributes little to the interaction (not shown). Distances between atoms of CDR2 residue H54Asn and Asn-983 and Trp-982 of the A3-domain are too long (3.7 and 3.8 Å, respectively) to qualify as hydrogen bonds. Moreover, only one residue of CDR2, H50Trp, is involved in hydrophobic contacts with the A3-domain, more specifically with Met-1022 and His-1023.

Interacting residues of the light chain (Fig. 2*C*) are mainly located in CDR2. CDR2 residue L49His forms a salt bridge with A3-domain residue Asp-1009, and L56Pro makes hydrophobic contacts with Ile-975. In CDR3, L95Arg makes hydrophobic contacts with Met-1022, and a rather long salt bridge is formed between L92Asp and Arg-1016 of the A3-domain. The only interaction between CDR1 of the light chain and the A3-domain is a hydrophobic interaction between L32Tyr and Arg-1016, respectively.

Paratope Definition Using Alanine Mutants of scFv-82D6A3(WT)—To define more precisely the role of individual amino acids of 82D6A3 in binding to VWF-A3, we constructed alanine mutants of 82D6A3 and measured their interaction with VWF. Because, as previously reported (52), the scFv of 82D6A3 binds to VWF and inhibits its interaction with collagen, the DNA coding for this antibody fragment was used for the construction of the alanine mutants. We mutated all 82D6A3 residues that form hydrogen bonds or salt bridges with residues of the A3-domain (Table 3) as well as residues that are located within 4.0 Å of the A3-domain and have a buried solvent-accessible surface area in the complex of at least 20 Å^2. A total of thirteen residues were mutated to alanine, eight in the heavy chain (H31Asn → Ala, H32Tyr → Ala, H50Trp → Ala, H54Asn → Ala, H99Asp → Ala, H101Pro → Ala, H102Tyr → Ala, and H103Tyr → Ala) and five in the light chain (L32Tyr → Ala, L49His → Ala, L56Pro → Ala, L92Asp → Ala, L95Arg → Ala). All mutated proteins were expressed in *E. coli* HB2151 cells. Expression levels varied between 84 and 103% of the expression level obtained with scFv-82D6A3(WT) (data not shown). All proteins were subsequently purified from the supernatant and periplasmic extract to >90% purity (Fig. 3). Next, the effect of the individual mutations on the binding of the scFv to VWF was studied by enzyme-linked immunosorbent assay (Fig. 4). Except for H54Asn → Ala, all mutations in the heavy chain of 82D6A3 substantially decrease the affinity for VWF (Fig. 4*A*). Mutations in the light chain, however, only have a moderate, or no, effect on binding (Fig. 4*B*). Moreover, the binding of wild type and mutant scFv-82D6A3 to VWF was inhibited by IgG-82D6A3 (data not shown), proving the specificity of the binding.

Classification of mutants on the basis of their residual binding to VWF reveals that mutations with a strong effect on binding (<40% residual binding compared with WT) form a continuous patch in the center of the antigen binding surface (Figs. 4*C* and 5). This class contains mutants H31Asn → Ala (18.2 ± 1.6%), H32Tyr → Ala (28.7 ± 2.6%), H99Asp → Ala (1.9 ± 0.3%), H101Pro → Ala (38.3 ± 1.3%), H102Tyr → Ala (13.3 ± 3.7%), and H103Tyr → Ala (15.5 ± 4.5%), which are all located either in CDR1 or in CDR3 of the heavy chain. A

TABLE 3
Hydrogen bonds and salt bridges between 82D6A3 and the VWF A3-domain

82D6A3				A3-domain[a]			Interaction[b] Distance (Å)
Amino acid	Position[c]	CDR[d]	Atom	Amino acid	Position[e]	Atom	
Asn	H31	1	ND2	Ile	978	O	3.0
Asn	H31	1	ND2	Asp	979	O	3.3
Tyr	H32	1	OH	Ile	978	N	2.9
Asp	H99	3	OD2	**His**	**1023**	NE2	2.5*
Tyr	H103	3	OH	**Asp**	**1009**	OD2	2.6
Tyr	H103	3	OH	Thr	976	N	2.9
His	L49	2	NE2	**Asp**	**1009**	OD1	2.9*
Asp	L92	3	OD1	**Arg**	**1016**	NH1	3.4*

[a] Residues in the A3-domain previously reported as being part of the epitope are in bold (30).
[b] Hydrogen bonds (d ≤ 3.3 Å) and salt bridges (d ≤ 3.5 Å) between 82D6A3 and the A3-domain are listed. Salt bridges are indicated with *.
[c] Position of the residue in the 82D6A3 heavy (H) or light (L) chain (52).
[d] The CDR loop to which the residue belongs.
[e] Position of the residue in the A3-domain starting from the first amino acid of mature VWF.

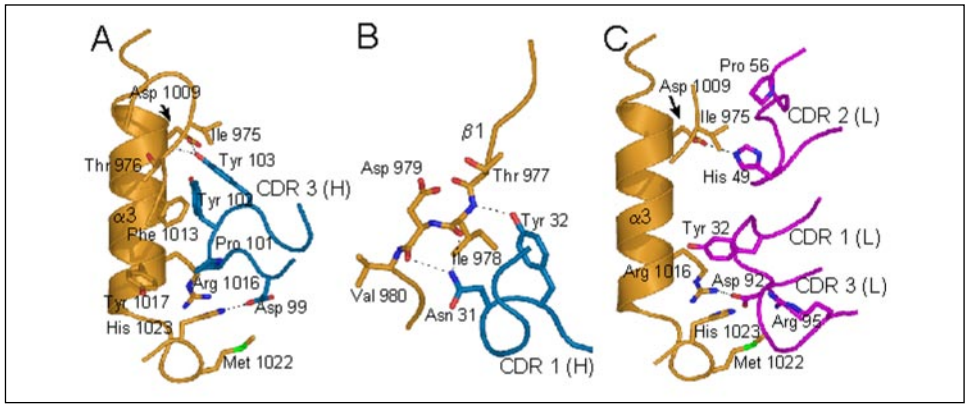

FIGURE 2. **Interactions between 82D6A3 and the VWF A3-domain.** Close-up views of CDRs and interacting regions of the A3-domain. Residues that have intermolecular contacts closer than 4 Å are depicted in *stick* representation. Hydrogen bonds and salt bridges are shown as *dashed lines*. *Coloring* of ribbons and loops is identical to Fig. 1*A*.

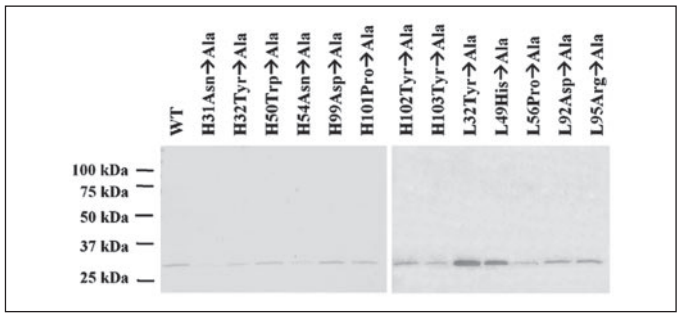

FIGURE 3. **Expression of scFv-82D6A3 and its mutants.** The scFv-82D6A3 and its alanine mutants were expressed in *E. coli* HB2151 cells and purified from the supernatant and periplasm by affinity chromatography on a HiTrap anti-E Tag column. Equal volumes of the elution fractions were loaded on a 10% SDS-PAGE gel, and purity was checked by staining with Coomassie Brilliant Blue.

second class of mutants with a moderate effect on binding (40–80% residual binding) contains H50Trp → Ala (65.2 ± 2.5%) and L49His → Ala (75.8 ± 1.3%) (Fig. 4*C*). On the molecular surface these residues are connected to the perimeter of the central cluster (Fig. 5). Located at the periphery of the surface formed by residues with a strong or moderate effect on binding is a third class of residues that have little or no effect (80–100% residual binding) (Fig. 5). This class contains H54Asn → Ala (99.0 ± 0.74%), L32Tyr → Ala (93.7 ± 6.4), L56Pro → Ala (87.2 ± 4.5%), L92Asp → Ala (91.7 ± 0.28%), and L95Arg (89.3 ± 4.2%) (Fig. 4*C*). Except for H54Asn → Ala, these are all located in the light chain. In summary, these data reveal that the paratope of 82D6A3 predominantly consists of heavy chain residues from two short linear sequences in CDR1 (H31Asn, H32Tyr) and CDR3 (H99Asp, H101Pro, H102Tyr, H103Tyr) with residues H50Trp and L49His playing ancillary roles (Fig. 5).

DISCUSSION

Inhibitors of the interaction of VWF with collagen types I and III as new antithrombotic compounds can have important advantages over currently used antithrombotic agents, such as GPIIbIIIa antagonists. Because the VWF-collagen interaction only mediates platelet adhesion and thrombus formation in high shear stress conditions, overall hemostasis is only minimally affected by inhibition of this interaction, which might result in a reduced risk for bleeding complications. Moreover, by interfering with the first step in primary hemostasis, inhibitors of the VWF-collagen interaction also prevent platelet activation, a process that mediates intimal hyperplasia after angioplasty or endarterectomy by the release of smooth muscle cell-proliferating and -attracting factors (34, 54).

Indeed, previous *in vivo* studies demonstrated that 82D6A3, a monoclonal antibody that inhibits the VWF-collagen interaction through binding to the VWF A3-domain, is a powerful antithrombotic agent. Importantly, administration of 82D6A3 did not significantly prolong the bleeding time, even at high doses (31). To maximally exploit the *in vivo* effects of 82D6A3, developing an orally active compound with the same characteristics as the monoclonal antibody is a prerequisite. As a first step in the development of such a new antithrombotic peptidomimetic related to 82D6A3, we determined its paratope by resolving the crystal structure of the complex between a Fab fragment of 82D6A3 and the VWF A3-domain combined with mutagenesis studies.

The crystal structure of the complex shows that most of the A3 residues previously reported as being part of the epitope (Arg-963, Pro-981, Asp-1009, Arg-1016, Ser-1020, Met-1022, and His-1023) (30) do indeed interact with 82D6A3. This is not true, however, for Ser-1020. Mutation of this residue to Ala affects binding to 82D6A3, but in the complex no

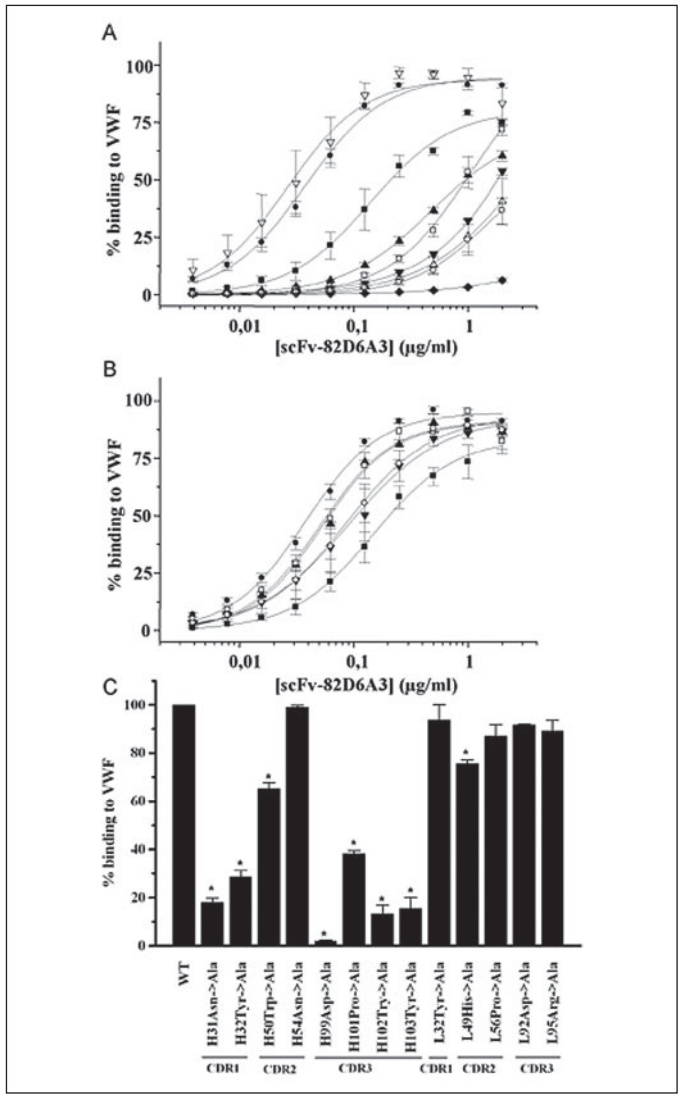

FIGURE 4. **Comparison of the VWF binding of scFv-82D6A3(WT) and its alanine mutants.** The concentration of purified scFvs was measured according to the Bradford method (53). Different concentrations of purified WT and mutant scFv-82D6A3 were added to VWF-coated wells, and bound scFv was detected with anti-E Tag-horseradish peroxidase antibodies. *A*, VWF binding of mutants containing mutations in the heavy chain of scFv-82D6A3 (▼, H31Asn → Ala; □, H32Tyr → Ala; ■, H50Trp → Ala; ▽, H54Asn → Ala; ♦, H99Asp → Ala; ▲, H101Pro → Ala; Δ, H102Tyr → Ala; ○, H103Tyr → Ala) (52) compared with the VWF binding of scFv-82D6A3(WT) (●). The maximal absorbance calculated from the fitted curve obtained with scFv-82D6A3(WT) was arbitrarily set to 100% binding. All curves were fitted to the Hill equation. *B*, VWF binding of mutants containing mutations in the light chain of scFv-82D6A3 (▲, H32Tyr → Ala; ■, H49His → Ala; ▼, L56Pro → Ala; ○, L92Asp → Ala; □, L95Arg → Ala) (52) compared with the VWF binding of scFv-82D6A3(WT) (●). The percentage of binding was calculated and is represented as described for the mutants of the heavy chain. *C*, percentage of binding to VWF of all mutants compared with scFv-82D6A3(WT) at 0.5 μg/ml, the concentration where maximal binding to VWF is obtained for scFv-82D6A3(WT). *, $p \leq 0.005$. All data points are the mean ± S.E. of single measurements in three independent experiments.

direct interactions involving this residue are observed. Apparently, Ser-1020 plays an indirect role in complex formation. It may do so by hydrogen bonding to His-1023, an important residue for 82D6A3 binding (30), thereby maintaining a conformation critical for recognition by 82D6A3. In addition, no direct interactions involving Arg-963 are observed in the complex, whereas mutation of this residue decreases the binding to 82D6A3. However, because the decrease in binding is subtle (25%) (30), this suggests a minor role in complex formation at most, which is now confirmed by the crystal structure. For Asp-979 the opposite is true. Mutation of this residue has no effect on binding, although it

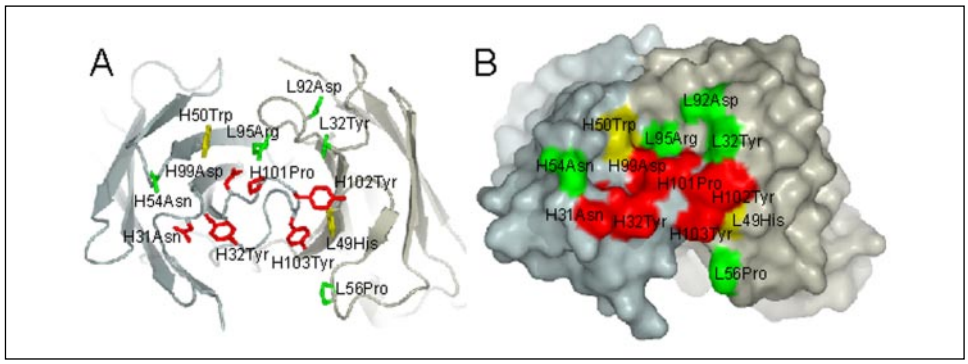

FIGURE 5. **The paratope of 82D6A3.** *A*, ribbon diagram of the variable domains of 82D6A3 with amino acids of the paratope shown in *stick* representation and colored according to the extent of residual VWF binding observed if mutated to alanine: 0–40%, *red*; 40–80%, *yellow*; 80–100%, *green*. *B*, surface representation of the variable domains of 82D6A3 with surfaces corresponding to residues in the paratope color coded as in *panel A*.

is involved in direct interactions with 82D6A3 residue H31Asn. This apparent discrepancy is explained by the fact that H31Asn hydrogen bonds to the main chain carbonyl of Asp-979, an interaction that is not affected by mutagenesis.

The epitope now observed in the crystal structure supports our previous conclusion from binding studies that the collagen and 82D6A3 binding sites on A3 overlap substantially (Fig. 1*C*) (30). A much smaller overlap with the putative collagen binding site is observed in the crystal structure of the VWF A3-domain bound to RU5 (27) (Protein Data Bank accession code 1FE8), an antibody that also inhibits collagen binding. Although 82D6A3 extensively interacts with the collagen binding face of A3, RU5 interacts with this face only to a very limited extent and predominantly engages the bottom face. Whereas the RU5 and 82D6A3 binding sites are distinctly different, both molecules, when bound to A3, do occupy a small common volume of space, which explains why they compete for binding to VWF.

On the basis of the crystal structure of the A3–82D6A3 complex we selected amino acids for mutagenesis to determine the paratope more precisely. Selection criteria used were involvement in an intermolecular salt bridge or hydrogen bond or a decrease in solvent-accessible surface area of >20 Å^2. The thirteen residues that were mutated account for ~85% of the total surface area of 82D6A3 buried in the complex. For mutagenesis, we used the scFv of 82D6A3, because the DNA coding for the scFv is much smaller and easier to handle than the DNA coding for the IgG. This is justified because the binding and inhibition characteristics of the scFv and the IgG are very similar (52). As the protein yield after purification was not the same for all mutants, despite the use of an anti-E Tag column, we cannot exclude that the alanine substitutions might have an influence on this. However, as the expression level of all mutants was comparable with that of scFv-82D6A3(WT) and varied between 84 and 103% of the expression level of scFv-82D6A3(WT), this indicates that the alanine substitutions did not markedly affect the structural integrity of the molecule by inducing global conformational changes. We studied the binding of the alanine mutants using full-length VWF instead of the A3-domain, because this is more physiologically relevant. In the binding studies we observed that 5 of 13 mutations tested do not affect VWF binding significantly, suggesting that our selection of residues has not been overly restrictive and that it likely includes all residues that contribute to the interaction significantly.

Residues identified as being essential for antigen binding are H31Asn, H32Tyr, H99Asp, H101Pro, H102Tyr, and H103Tyr. These residues are located in two loops and form one continuous patch on the surface of the antibody. H50Trp and L49His, situated adjacent to this patch, play ancillary roles in binding (Fig. 5).

Before we succeeded in resolving the crystal structure of the 82D6A3-A3-domain complex, we computationally determined the structure of the complex between the crystal structure of the VWF A3-domain (22) and the homology-modeled Fv-82D6A3 (52) using the automated docking program DOT (www.sdsc.edu/CCMS/DOT/). Interestingly, the position of 82D6A3 on the A3-domain in the obtained model corresponded strikingly well with the one in the co-crystal, implying that docking successfully predicted the overall structure of the 82D6A3-A3-domain complex. As a consequence, similar amino acids interacting with the A3-domain were identified both in the co-crystal and the docking model (H102Tyr, H103Tyr, L32Tyr, and L92Asp), of which two indeed turned out to be part of the paratope (H102Tyr and H103Tyr). Although the overall structure of the homology-modeled Fv-82D6A3, which was used in the docking procedure, corresponded well with the structure of the Fv-82D6A3 in the co-crystal, subtle differences in the conformation of the CDR loops were present. As a consequence, additional 82D6A3 residues interacting with the A3-domain were identified in the co-crystal.

The properties of the dominant region of the paratope, two short loops that form a continuous surface patch, are typical for antigen recognition segments of antibodies. Although it will be a challenge to construct a mimic peptide based on the paratope, techniques have been developed to mimic the tertiary structure of multiple loops in order to direct the critical amino acids into the same conformation and orientation as in the bio-active surface of the native protein (55, 56), and successful design of mimic peptides derived from CDRs has been reported (57, 58). The construction of such a peptide resembling the paratope in both charge distribution and conformation and investigation of its binding and inhibiting characteristics will be the next step in the development of an orally active antithrombotic compound with potentially important advantages over the existing antithrombotic agents.

Acknowledgments—We thank Dr. A. Gils and Dr. K. Verbeke for useful suggestions concerning the expression of scFvs. We acknowledge the European Synchrotron Radiation Facility for provision of synchrotron radiation.

REFERENCES

1. Sixma, J. J., van Zanten, G. H., Huizinga, E. G., van der Plas, R. M., Verkley, M., Wu, Y. P., Gros, P., and de Groot, P. G. (1997) *Thromb. Haemostasis* **78,** 434–438
2. Tschopp, T. B., Weiss, H. J., and Baumgartner, H. R. (1974) *J. Lab. Clin. Med.* **83,** 296–300
3. Savage, B., Saldivar, E., and Ruggeri, Z. M. (1996) *Cell* **84,** 289–297
4. Santoro, S. A. (1986) *Cell* **46,** 913–920
5. Kehrel, B., Wierwille, S., Clemetson, K. J., Anders, O., Steiner, M., Knight, C. G., Farndale, R. W., Okuma, M., and Barnes, M. J. (1998) *Blood* **91,** 491–499
6. Clemetson, K. J., and Clemetson, J. M. (2001) *Thromb. Haemostasis* **86,** 189–197
7. Clemetson, J. M., Polgar, J., Magnenat, E., Wells, T. N., and Clemetson, K. J. (1999) *J. Biol. Chem.* **274,** 29019–29024
8. Savage, B., Almus-Jacobs, F., and Ruggeri, Z. M. (1998) *Cell* **94,** 657–666
9. Shattil, S. J., Kashiwagi, H., and Pampori, N. (1998) *Blood* **91,** 2645–2657
10. Phillips, D. R., Charo, I. F., and Scarborough, R. M. (1991) *Cell* **65,** 359–362
11. Phillips, D. R., Charo, I. F., Parise, L. V., and Fitzgerald, L. A. (1988) *Blood* **71,** 831–843

12. Alberio, L., and Dale, G. L. (1998) *Br. J. Haematol.* **102,** 1212–1218
13. Sixma, J. J., Schiphorst, M. E., Verweij, C. L., and Pannekoek, H. (1991) *Eur. J. Biochem.* **196,** 369–375
14. Lankhof, H., van Hoeij, M., Schiphorst, M. E., Bracke, M., Wu, Y. P., Ijsseldijk, M. J., Vink, T., de Groot, P. G., and Sixma, J. J. (1996) *Thromb. Haemostasis* **75,** 950–958
15. Hoylaerts, M. F., Yamamoto, H., Nuyts, K., Vreys, I., Deckmyn, H., and Vermylen, J. (1997) *Biochem. J.* **324,** Pt. 1, 185–191
16. Mazzucato, M., Spessotto, P., Masotti, A., De Appollonia, L., Cozzi, M. R., Yoshioka, A., Perris, R., Colombatti, A., and De Marco, L. (1999) *J. Biol. Chem.* **274,** 3033–3041
17. Ross, J. M., McIntire, L. V., Moake, J. L., and Rand, J. H. (1995) *Blood* **85,** 1826–1835
18. Denis, C., Baruch, D., Kielty, C. M., Ajzenberg, N., Christophe, O., and Meyer, D. (1993) *Arterioscler. Thromb.* **13,** 398–406
19. Colombatti, A., and Bonaldo, P. (1991) *Blood* **77,** 2305–2315
20. Santoro, S. A., and Zutter, M. M. (1995) *Thromb. Haemostasis* **74,** 813–821
21. Perkins, S. J., Smith, K. F., Williams, S. C., Haris, P. I., Chapman, D., and Sim, R. B. (1994) *J. Mol. Biol.* **238,** 104–119
22. Huizinga, E. G., van der Plas, M., Kroon, J., Sixma, J. J., and Gros, P. (1997) *Structure* **5,** 1147–1156
23. Bienkowska, J., Cruz, M., Atiemo, A., Handin, R., and Liddington, R. (1997) *J. Biol. Chem.* **272,** 25162–25167
24. Emsley, J., King, S. L., Bergelson, J. M., and Liddington, R. C. (1997) *J. Biol. Chem.* **272,** 28512–28517
25. Kamata, T., and Takada, Y. (1994) *J. Biol. Chem.* **269,** 26006–26010
26. Kamata, T., Liddington, R. C., and Takada, Y. (1999) *J. Biol. Chem.* **274,** 32108–32111
27. Romijn, R. A., Bouma, B., Wuyster, W., Gros, P., Kroon, J., Sixma, J. J., and Huizinga, E. G. (2001) *J. Biol. Chem.* **276,** 9985–9991
28. Romijn, R. A., Westein, E., Bouma, B., Schiphorst, M. E., Sixma, J. J., Lenting, P. J., and Huizinga, E. G. (2003) *J. Biol. Chem.* **278,** 15035–15039
29. Nishida, N., Sumikawa, H., Sakakura, M., Shimba, N., Takahashi, H., Terasawa, H., Suzuki, E. I., and Shimada, I. (2003) *Nat. Struct. Biol.* **10,** 53–58
30. Vanhoorelbeke, K., Depraetere, H., Romijn, R. A., Huizinga, E. G., De Maeyer, M., and Deckmyn, H. (2003) *J. Biol. Chem.* **278,** 37815–37821
31. Wu, D., Vanhoorelbeke, K., Cauwenberghs, N., Meiring, M., Depraetere, H., Kotze, H. F., and Deckmyn, H. (2002) *Blood* **99,** 3623–3628
32. Sadler, J. E. (2002) *Blood* **99,** 3491
33. Barnes, C. S., Krafft, B., Frech, M., Hofmann, U. R., Papendieck, A., Dahlems, U., Gellissen, G., and Hoylaerts, M. F. (2001) *Semin. Thromb. Hemostasis* **27,** 337–348
34. Cruz, C. P., Eidt, J., Drouilhet, J., Brown, A. T., Wang, Y., Barnes, C. S., and Moursi, M. M. (2001) *J. Vasc. Surg.* **34,** 724–729
35. Cauwenberghs, N., Meiring, M., Vauterin, S., van Wyk, V., Lamprecht, S., Roodt, J. P., Novak, L., Harsfalvi, J., Deckmyn, H., and Kotze, H. F. (2000) *Arterioscler. Thromb. Vasc. Biol.* **20,** 1347–1353
36. Wu, D., Meiring, M., Kotze, H. F., Deckmyn, H., and Cauwenberghs, N. (2002) *Arterioscler. Thromb. Vasc. Biol.* **22,** 323–328
37. Kageyama, S., Yamamoto, H., Nagano, M., Arisaka, H., Kayahara, T., and Yoshimoto, R. (1997) *Br. J. Pharmacol.* **122,** 165–171
38. Kageyama, S., Yamamoto, H., Nakazawa, H., and Yoshimoto, R. (2001) *Thromb. Res.* **101,** 395–404
39. Reilly, I. A., and FitzGerald, G. A. (1988) *Drugs* **35,** 154–176
40. The EPIC Investigators (1994) *N. Engl. J. Med.* **330,** 956–961
41. Trivedi, S. M., Shani, J., and Hollander, G. (2002) *J. Invasive Cardiol.* **14,** 423–425
42. Ferns, G. A., Raines, E. W., Sprugel, K. H., Motani, A. S., Reidy, M. A., and Ross, R. (1991) *Science* **253,** 1129–1132
43. Lindner, V., and Reidy, M. A. (1991) *Proc. Natl. Acad. Sci. U. S. A.* **88,** 3739–3743
44. Collaborative Computational Project Number 4 (1994) *Acta Crystallogr. Sect. D Biol. Crystallogr.* **50,** 760–763
45. Leslie, A. G. W. (1992) *Joint CCP4 + ESF-EAMCB Newsletter on Protein Crystallography 26*
46. Brunger, A. T., Adams, P. D., Clore, G. M., DeLano, W. L., Gros, P., Grosse-Kunstleve, R. W., Jiang, J. S., Kuszewski, J., Nilges, M., Pannu, N. S., Read, R. J., Rice, L. M., Simonson, T., and Warren, G. L. (1998) *Acta Crystallogr. Sect. D Biol. Crystallogr.* **54,** Pt. 5, 905–921
47. van den Elsen, J. M., Herron, J. N., Hoogerhout, P., Poolman, J. T., Boel, E., Logtenberg, T., Wilting, J., Crommelin, D. J., Kroon, J., and Gros, P. (1997) *Proteins* **29,** 113–125
48. Perrakis, A., Morris, R., and Lamzin, V. S. (1999) *Nat. Struct. Biol.* **6,** 458–463
49. Zou, J. Y., and Jones, T. A. (1996) *Acta Crystallogr. Sect. D Biol. Crystallogr.* **52,** 833–841
50. Murshudov, G. N., Vagin, A. A., and Dodson, E. J. (1997) *Acta Crystallogr. Sect. D Biol. Crystallogr.* **53,** 240–255
51. Winn, M. D., Isupov, M. N., and Murshudov, G. N. (2001) *Acta Crystallogr. Sect. D Biol. Crystallogr.* **57,** 122–133
52. Staelens, S., Desmet, J., Ngo, T. H., Vauterin, S., Pareyn, I., Barbeaux, P., Van Rompaey, I., Stassen, J. M., Deckmyn, H., and Vanhoorelbeke, K. (2006) *Mol. Immunol.*, in press
53. Bradford, M. M. (1976) *Anal. Biochem.* **72,** 248–254
54. Ferns, G. A., and Avades, T. Y. (2000) *Int. J. Exp. Pathol.* **81,** 63–88
55. Fairlie, D. P., West, M. L., and Wong, A. K. (1998) *Curr. Med. Chem.* **5,** 29–62
56. Eichler, J. (2004) *Protein Pept. Lett.* **11,** 281–290
57. Feng, J., Li, Y., Zhang, W., and Shen, B. (2005) *Immunol. Lett.* **98,** 311–316
58. Doring, E., Stigler, R., Grutz, G., von Baehr, R., and Schneider-Mergener, J. (1994) *Mol. Immunol.* **31,** 1059–1067